Topology-Dependent Communication and Computing in Bioengineered Neuronal Networks

Joshua Mullett, Andrea Mohr, Reinhold Scherer, *Senior Member, IEEE,* and Michael T. Barros, *Senior Member, IEEE*

***Abstract*—Bioengineered neuronal systems are increasingly explored as living computational substrates, yet their end-to-end communication properties remain poorly characterized beyond global activity statistics. We model a mechanosensitive spiking neuronal network as a noisy multiple-input multiple-output (MIMO) communication system to quantify how topology and substrate mechanics shape information transfer and computation. Using a mechanosensitive Izhikevich network with time-varying stiffness, we compare random, clustered, and disintegrated topologies under matched stimulation and observation noise. Communication is quantified using transfer entropy, achievable mutual information rate from binned spike observations, and information redundancy. Computation is evaluated using a receiver-level separability metric posed as a transmitter-identification task. Across noise levels, clustered networks more consistently maintain higher achievable rates and exhibit more concentrated transmitter–receiver separability than random and disintegrated substrates. These results show that topology and mechanical state jointly regulate communication and computational separability in bioengineered neuronal networks, providing design-relevant metrics for bioengineered intelligence systems.**

***Index Terms*—Bioengineered intelligence, spiking neuronal networks, transfer entropy, mutual information, co-information, decoding, network topology.**

I. Introduction

Advances in biofabrication and neuronal engineering have renewed interest in using living neuronal networks as computational and communication substrates, ranging from in vitro cultures interfaced with multi-electrode arrays to bioengineered systems with partially controlled geometry and connectivity [1], [2], [3]. Controlled topology, modularity, and patterned growth are known to shape emergent activity, bursting dynamics, and functional organization in vitro [4], [3], [5], [6]. Cortical microcircuits also exhibit non-random clustered connectivity [7]. However, engineered neuronal substrates are still commonly evaluated using global activity measures such as firing rate, bursting, or synchronization, which provide limited insight into how information is routed, preserved, or separated under noisy interface-limited observation.

Existing neuronal communication models often focus on information-rate estimation, stimulus reconstruction, or graph-theoretic measures of effective connectivity. These approaches are valuable for linking activity statistics to functional structure, but they often (i) rely on assumptions such as stationarity, linearity, or low-order dependence that can be restrictive in recurrent spiking networks, and (ii) treat the channel as neuron-to-neuron signaling rather than an operational end-to-end interface between stimulation and recording [8], [9], [10], [11], [12], [13]. In bioengineered networks, stimulation and readout are mediated by physical interfaces, such as electrodes or optogenetic regions of interest, so performance assesses in terms of what a receiver can infer from observable spike activity. This motivates a communication-theoretic formulation in which topology, mechanics, and interface placement jointly condition the effective biological channel.

Noisy neuronal network is a directed system in which spikes act as symbols and network topology constrains the available pathways for signal propagation. Under this view, the key question is not merely whether neurons respond to stimulation, but whether the network supports reliable and differentiable information transfer between spatially separated regions under realistic constraints. This distinction is especially relevant for bioengineered intelligence systems, where stimulation and readout are constrained by physical interfaces rather than arbitrary neuron-level access. Despite growing interest in structured neuronal substrates, the relationship between network topology and communication performance in spatially embedded systems remains poorly understood. In particular, it is unclear how randomness, clustering, or structural degradation shape directed information transfer, robustness to synaptic noise, and channel differentiation over long spatial distances. That also impacts the quantification of computing performance, which is tied by how information propagates under noisy channels in neuronal networks.

Here, we investigate how network topology modulates communication and computing in bioengineered neuronal substrates under noise and stiffness modulation. Using a mechanosensitive neuronal network model with a time-varying substrate stiffness, we compare random, clustered, and disintegrated topologies under matched stimulation and symbol-level spike-noise. Fig. 1 depicts our methods. We quantify directed transfer entropy [14], achievable mutual information rate derived from binned spike observations [15], and information redundancy. To quantify network computation, we also evaluate receiver-level separability as a transmitter-identification proxy under TX/RX placement constraints. Our methodology links structure, mechanosensitivity, and interface-limited decoding to design-relevant metrics for bioengineered intelligence.

II. Neuronal Bioengineered Communication Network Model

The proposed framework models the neuronal substrate as a directed, time-varying graph $\mathcal{G} = (\mathcal{V}, \mathcal{E}, W)$, where $\mathcal{V}$ denotes the set of N neurons and $W \in \mathbb{R}^{N\times N}$ represents the synaptic efficacy matrix. The system state at time t is defined by the membrane potential vectors $\mathbf{v}(t)$ and recovery variables $\mathbf{u}(t)$, evolved via hybrid non-linear differential equations. A distinctive feature of this methodology is the coupling of electrophysiological dynamics with a mechanobiological operator $\Phi(S, v)$, where S represents extracellular stiffness. The system is driven by a stochastic external forcing func-

JM, RS and MB are with the School of Computer Science and Electronic Engineering, University of Essex, UK.

AM is with the School of Life Sciences, University of Essex, UK.

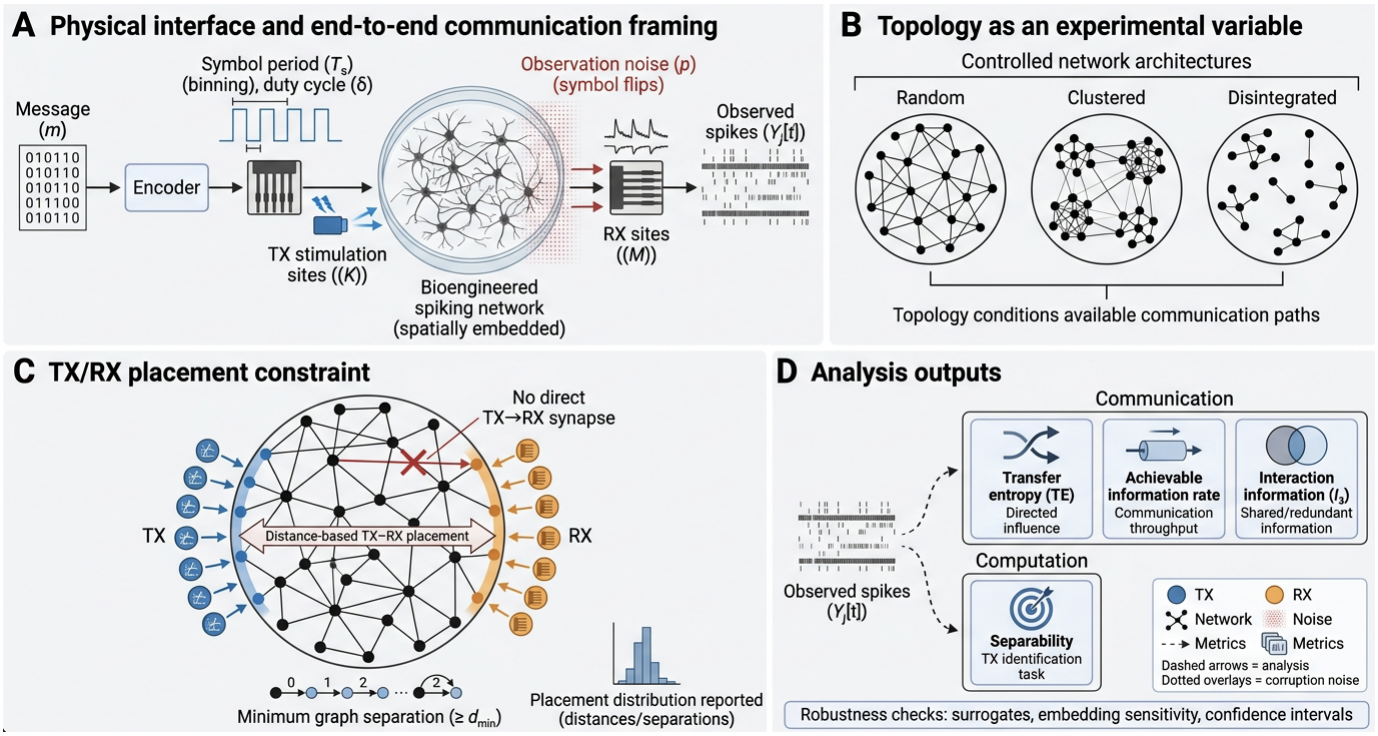

Fig. 1: Bioengineered neuronal substrates as interfaced communication systems. (A) TX interfaces deliver encoded inputs, (B) random, clustered, or disintegrated networks transform them, (C) RX interfaces record noise-corrupted binned spikes, and (D) TE, achievable MI rate, and TX separability quantify communication performance.

tion $\mathbf{I}_{ext}(t)$, and the network evolves under the influence of local Hebbian plasticity rules ($\mathcal{H}$) and global homeostatic constraints ($\mathcal{R}$), effectively solving the tuple $(\mathcal{G}, \mathbf{v}, \mathbf{u}, W, S)$ via Euler integration.

A. System Model (TX/RX, Interface, and Objective)

We interpret the substrate as a physically interfaced multiple-input multiple-output (MIMO) communication system. Let $\mathcal{T} = \{1, \ldots, K\}$ denote a set of K transmitters (TX sites) and $\mathcal{R} = \{1, \ldots, M\}$ denote a set of M receivers (RX sites), instantiated as stimulation and recording interfaces (e.g., electrode contacts or optogenetic regions of interest) that couple to subsets of neurons, consistent with emerging molecular and exosome-mediated biological communication channel models [16], [17]. A message $m \in \{1, \ldots, 2^{nR}\}$ is mapped by an encoder into a length-n symbol sequence $\mathbf{x}^n \in \mathcal{X}^n$ over a binary input alphabet $\mathcal{X} = \{0, 1\}$, with symbol period T_s and duty cycle $\delta \in (0, 1]$.

Encoding rule. A TX symbol $x_t \in \{0, 1\}$ is embedded into stimulation by amplitude-shift keying: during each symbol interval $[tT_s, (t+1)T_s)$, a square-wave current of duration δT_s is applied with amplitude A_1 if $x_t = 1$ and A_0 if $x_t = 0$, while all other stimulation parameters (symbol period T_s, duty cycle δ, and interface placement) are held fixed across experiments.

Observation and decoding rule. The receiver does not observe membrane states; instead, each RX observes a binned spike-count (or binary spike) process $Y_j[t]$ obtained by spike detection within the interface's capture region, followed by optional symbol-level corruption noise. A decoder $\hat{m} = g(\mathbf{Y}^n)$ (or, for the separability task, $\hat{i} = g_j(\mathbf{Y}_j^n)$) maps observed RX sequences to a message (or to the most likely intended transmitter). The operational objective is reliable end-to-end communication under physical constraints: maximize achievable information rate and transmitter identifiability subject to fixed stimulation energy, topology, and observation noise.

B. Network Topology and Graph Construction

The neuronal network is initialized as a spatial graph of N neurons with two-dimensional positions $p_i \in \mathbb{R}^2$. Connectivity is determined using a probabilistic adjacency matrix to capture biologically constrained spatial organization. To examine how topology influences communication, we consider random, clustered, and disintegrating networks. Random networks use distance-constrained probabilistic connectivity, clustered networks contain locally dense subnetworks with sparse inter-cluster coupling, and disintegrating networks model progressive structural degradation through edge pruning.

For clustered topologies, neurons are assigned to cluster centers C_k such that the connection probability between neurons i and j depends on cluster identity:

$$P_{ij} = \begin{cases} \rho_{\text{intra}}, & C(i) = C(j) \\ \rho_{\text{inter}}, & C(i) \in \mathcal{N}(C(j)) \\ 0, & \text{otherwise} \end{cases} \tag{1}$$

where $C(i)$ denotes the cluster assignment of neuron i, $\mathcal{N}(\cdot)$ neighboring clusters, and ρ the connection density.

To simulate structural degradation, edges are pruned based on Euclidean distance $d_{ij} = \|p_i - p_j\|_2$. An edge (i, j) is removed with probability

$$P_{\text{prune}}(i, j) = \lambda_{\text{prune}}(1 + d_{ij}), \tag{2}$$

where λ_{prune} is the disintegration factor.

C. Biomechanical Neuron Model

The neuronal dynamics follow the Izhikevich formalism [18], [19], augmented by a novel mechanotransduction current. Neuron-specific variables are indexed by $i \in \{1, \ldots, N\}$.

The state variables v_i (membrane potential) and u_i (recovery variable) evolve according to:

$$\frac{dv_i}{dt} = 0.04v_i^2 + 5v_i + 140 - u_i + I_{total,i}(t), \tag{3}$$

$$\frac{du_i}{dt} = a_i(b_i v_i - u_i), \tag{4}$$

where a_i, b_i determine the timescale and sensitivity of the recovery variable. The reset condition upon spiking ($v_i \geq 30$ mV) is defined as:

$$\text{if } v_i \geq 30 \text{ mV, then } \begin{cases} v_i \leftarrow c_i \\ u_i \leftarrow u_i + d_i \end{cases} \tag{5}$$

The total current $I_{\text{total},i}$ is the sum of synaptic, external, and mechanical components:

$$I_{\text{total},i}(t) = g_i(t)I_{\text{syn},i}(t) + I_{\text{mech},i}(t) + I_{\text{ext},i}(t) + \xi(t) \tag{6}$$

where $g_i(t)$ is an intrinsic gain factor and $\xi(t) \sim \mathcal{N}(\mu_\xi, \sigma_\xi^2)$, where μ_ξ and σ_ξ denote the mean and standard deviation of the background current noise, respectively.

The mechanotransduction current $I_{\text{mech},i}$ models the neuron's response to environmental stiffness S (in kPa) [20], [21]. We define a Hill-type modulation factor $M(S)$ and an adhesion coefficient $\alpha(S)$:

$$M(S) = I_{\max} \frac{K_{\text{half}}^h}{K_{\text{half}}^h + S^h}, \tag{7}$$

$$\alpha(S) = \beta_{\min} + \frac{\beta_{\max} - \beta_{\min}}{1 + e^{-(S-\theta_S)\cdot k_S}}, \tag{8}$$

where $h = 3.5$ is the Hill coefficient and $K_{\text{half}} = 40$ represents the half-maximal stiffness.

The resulting current is rectified relative to the resting potential ($E_{\text{rest}} = -65$ mV):

$$I_{\text{mech},i}(t) = \gamma \cdot \alpha(S) \cdot M(S) \cdot \max(0, v_i(t) - E_{\text{rest}}). \tag{9}$$

This model links extracellular mechanics (S) to intracellular excitability via the gain γ and adhesion strength α.

D. External Stimulation and Noise Models

The network is driven by an external current vector $\mathbf{I}_{\text{ext}}(t)$. While deterministic inputs (DC, Step) are supported, stochastic dynamics are modeled using an Ornstein-Uhlenbeck (OU) process to simulate synaptic background noise or fluctuating sensory input:

$$dx(t) = \theta_{\text{ou}}(\mu_{\text{ou}} - x(t))dt + \sigma_{\text{ou}}\sqrt{dt}\mathcal{N}(0,1), \tag{10}$$

$$I_{\text{ext},i}(t) = \mathcal{M}_i \cdot x(t), \tag{11}$$

where θ_{ou} is the reversion rate, σ_{ou} is the volatility , and $\mathcal{M}$ is a binary mask vector determining which neuronal groups receive input.

E. Information-Theoretic and Computational Metrics

To evaluate the network's performance as a reliable biocomputing substrate, we model the system as a Multiple-Input Multiple-Output (MIMO) communication channel.

1) Transfer Entropy (TE)

To measure the directed, causal influence from an input neuron spike train X to an output neuron spike train Y, we calculate the Transfer Entropy $T_{X\to Y}$. TE captures the reduction in uncertainty of the communication system, defined by:

$$T_{X\to Y} = H(Y_t \mid Y_{t-1:t-L}) - H(Y_t \mid Y_{t-1:t-L}, X_{t-1:t-L}), \tag{12}$$

where $H(\cdot)$ denotes Shannon entropy, Y_t is the state of the target at time t, and $X_{t-1:t-L}$ represents the history of the source over a lag window L.

2) Channel Capacity with Noisy Synapses

We define the channel capacity C as the intrinsic upper bound on information transmission rates given the network's noise profile. Modeling the synaptic transmission as a Binary Symmetric Channel (BSC) with an error probability p_e [8], [9], [12] (representing synaptic failure or spurious spiking), the theoretical capacity per spike bin is:

$$C_{BSC} = 1 - H_2(p_e) = 1 - (-p_e \log_2 p_e - (1-p_e)\log_2(1-p_e)), \tag{13}$$

where $H_2(\cdot)$ is the binary entropy function. Practically, capacity becomes:

$$C_{net} = \max_{P(X)} \sum_{x\in\mathcal{X}} \sum_{y\in\mathcal{Y}} P(x,y) \log_2 \left(\frac{P(x,y)}{P(x)P(y)} \right). \tag{14}$$

For completeness, we define the redundancy among an input X and two outputs $\{Y_1, Y_2\}$:

$$I_3(X; Y_1; Y_2) = I(X; Y_1) + I(X; Y_2) - I\big(X; \{Y_1, Y_2\}\big). \tag{15}$$

where I_3 represents the usual information-centric score of repeated information between TX/RX.

3) Operational Separability (TX Identification)

We define separability as receiver j identify the intended transmitter $i \in \mathcal{T}$ among K candidates from its observed spike train. For each receiver j, we compute a mutual-information-based separability score

$$S_j = \frac{I(X_{i^\star}; Y_j)}{\sum_{k\in\mathcal{T}} I(X_k; Y_j)}, \tag{16}$$

where $i^\star$ denotes the intended transmitter for receiver j under the placement rule.

III. Results

We simulated $N = 1000$ Izhikevich neurons for $T = 5000$ ms with timestep $\Delta t = 1$ ms and synaptic delay of 3 ms. Unless otherwise stated, plasticity mechanisms were disabled. Communication used $K = M = 30$ transceivers with binary amplitude-shift keyed stimulation ($A_1 = 15$, $A_0 = 0$) and symbol period $T_s = 10$ ms (bin size), matching the analysis window for information estimation. Substrate stiffness was stepped from $S = 5$ kPa to $S = 20$ kPa during the trial; all information-theoretic results were computed on binned spike observations after symbol-level corruption noise with flip probability $p \in \{0, 0.1, 0.2, 0.3, 0.4, 0.5\}$.

Spike trains were initially discretized using bins of width $\Delta = 5$ ms. Since the stimulation symbol period was $T_s = 10$ ms, each symbol interval contained two spike bins. For information-theoretic estimation, the spike observations were aligned to these 10 ms symbol intervals, yielding $n = T/T_s = 500$ symbol-level observations per trial. Transfer entropy was estimated using the discrete plug-in estimator, with an embedding length of $L = 3$ symbol intervals for the source and target histories, with a 30 ms history window. The lag was selected by maximizing $T_{X\to Y}(\tau)$ over $\tau \in 0, \ldots, 5$ symbol intervals. Mutual information and achievable rate were estimated from the same symbol-aligned observations using

TABLE I: Simulation and stimulation parameters.

Parameter	Value
Neuron count N	1000
Simulation time T	5000 ms
Integration timestep Δt	1 ms
Synaptic delay	3 ms
Stiffness protocol	step $5 \rightarrow 20$ kPa
TX/RX counts (K, M)	(30, 30)
Stimulation amplitudes (A_0, A_1)	(0, 15)
Noise levels p	$\{0, 0.1, 0.2, 0.3, 0.4, 0.5\}$
Replicates per p	20
Base random seed	42
Information-estimation settings	**Value**
Bin size / symbol period T_s	10 ms
Sample length n	500 symbols
TE embedding length L	3 bins
TE lag search	$\tau \in \{0, \ldots, 5\}$ bins
Estimator	discrete plug-in
Bias correction (MI/TE)	Miller–Madow (MI); none (TE)
Uncertainty	s.e. over 20 noise realizations

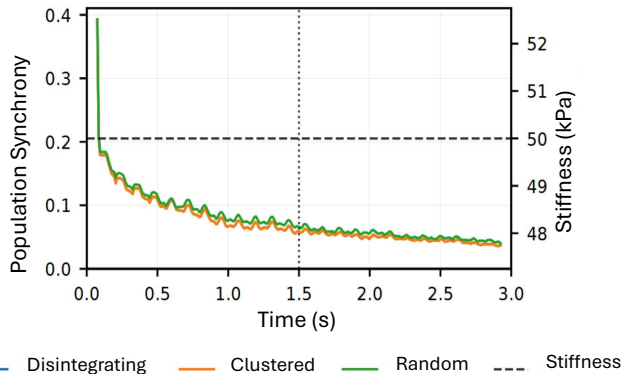

Fig. 2: Smoothed population synchrony under square-wave stimulation at constant substrate stiffness ($S = 50$ kPa).

the plug-in estimator with Miller–Madow bias correction. Estimates were aggregated over 20 runs per topology. All simulations used the same network construction seed (42) per topology and report variability over noisy rus. Parameter settings are summarized in Tables I.

A. Network Response under Stiffness Modulation

Fig. 2 shows the smoothed population synchrony under square-wave stimulation for random, clustered, and disintegrated network topologies at constant substrate stiffness ($S = 50$ kPa). All topologies exhibit stable collective synchrony dynamics under the mechanosensitive neuronal model, demonstrating that the network maintains coherent population-level activity across different connectivity organizations. This provides a consistent dynamical baseline for the communication-theoretic analysis presented in Fig. III-A.

B. Information Transfer and Redundancy under Noise

Fig. III-A(a) and Fig. III-A(b) show end-to-end communication under symbol-level spike-observation noise for random, clustered, and disintegrated topologies. Transfer entropy and achievable mutual information rate decrease with increasing corruption probability, consistent with progressive degradation of the observed spike symbols. The clustered topology maintains higher achievable mutual information across noise levels, indicating that modular connectivity can preserve more stimulus-related information at the receiver interface. Fig. III-A(c) shows the redundancy between transmitter and receiver observations. Higher redundancy in the clustered topology indicates that information is repeated across multiple receiver channels rather than being distributed independently, which is consistent with locally shared pathways within clustered subnetworks.

C. Biocomputing Separability

Fig. 4(a)–(c) show receiver-level separability matrices for the three topology classes. Larger values indicate that a receiver carries more information about a specific transmitter, meaning whether RX j can distinguish its intended TX from the other $K - 1$ candidates. The clustered topology produces a more concentrated TX→RX structure, showing that modular pathways preserve transmitter identity more clearly at the receiver level. Random networks produce more diffuse mappings, while disintegrated networks show fragmented mappings caused by loss of long-range communication paths. These results indicate that topology affects not only total information transfer, but also the separability of communication channels available for computation.

IV. Conclusion

We analyzed how network topology conditions information-routing structure in spatially embedded, bioengineered neuronal substrates under noise and stiffness modulation. Across conditions, transfer entropy and achievable mutual information decrease with increasing noise, but clustered networks more consistently maintain higher rates and show more concentrated transmitter–receiver (separability) mappings. In contrast, random networks appear less sensitive to stiffness changes, whereas more structured topologies exhibit stronger stiffness-dependent changes in propagation and synchrony. Together, these results show that controlled topology and placement constraints reveal design-relevant trade-offs between information transfer, redundancy, and separability, providing a quantification of topology structures of neural networks for bioengineered intelligence [13].

References

[1] B. J. Kagan, "Two roads diverged: Pathways toward harnessing intelligence in neural cell cultures," *Cell Biomaterials*, vol. 1, no. 8, p. 100156, 9 2025.

[2] M. T. Barros, P. Doan, M. Kandhavelu, B. Jennings, and S. Balasubramaniam, "Engineering calcium signaling of astrocytes for neural–molecular computing logic gates," *Scientific Reports 2021 11:1*, vol. 11, no. 1, pp. 595–, 1 2021.

[3] H. Lee, G. S. Yi, and Y. Nam, "Connectivity and network burst properties of in-vitro neuronal networks induced by a clustered structure with alginate hydrogel patterning," *Biomedical Engineering Letters*, vol. 13, no. 4, p. 659, 11 2023.

[4] E. Marconi, T. Nieus, A. Maccione, P. Valente, A. Simi, M. Messa, S. Dante, P. Baldelli, L. Berdondini, and F. Benfenati, "Emergent functional properties of neuronal networks with controlled topology," *PLoS ONE*, vol. 7, no. 4, 4 2012.

[5] M. Shein-Idelson, E. Ben-Jacob, and Y. Hanein, "Engineered neuronal circuits: A new platform for studying the role of modular topology," *Frontiers in Neuroengineering*, vol. 4, p. 10, 2011.

[6] J. H. Downes, M. W. Hammond, D. Xydas, M. C. Spencer, V. M. Becerra, K. Warwick, B. J. Whalley, and S. J. Nasuto, "Emergence of a small-world functional network in cultured neurons," *PLoS Computational Biology*, vol. 8, no. 5, p. e1002522, 2012.

[7] R. Perin, T. K. Berger, and H. Markram, "A synaptic organizing principle for cortical neuronal groups," *Proceedings of the National Academy of Sciences*, vol. 108, no. 13, pp. 5419–5424, 3 2011.

[8] M. Veletić and I. Balasingham, "Capacity estimation in mimo synaptic channels," in *Proceedings of the 5th ACM International Conference on Nanoscale Computing and Communication*, ser. NANOCOM '18. New York, NY, USA: Association for Computing Machinery, 2018.

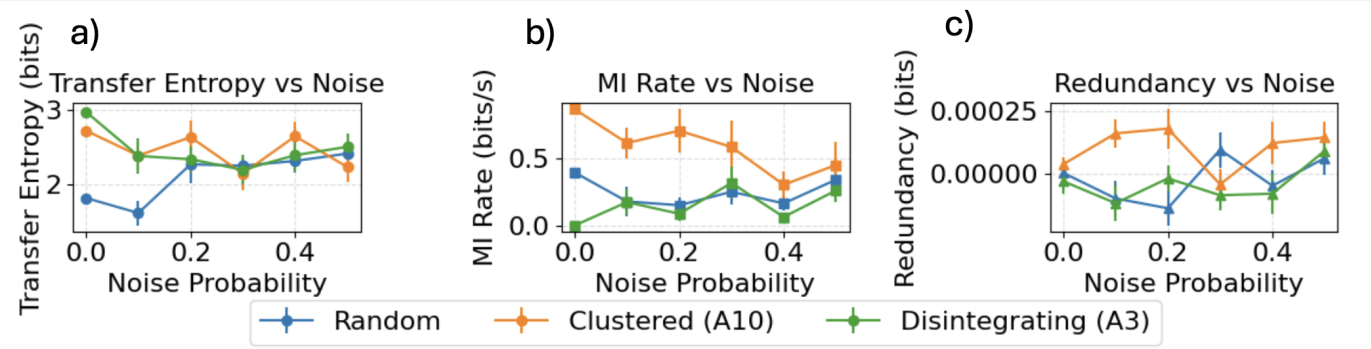

Fig. 3: Topology-dependent communication performance under increasing spike-observation noise. (a) Transfer entropy (TE), (b) achievable mutual information rate, and (c) receiver-channel redundancy, quantified using $I_3(X;Y_1;Y_2)$, for random, clustered, and disintegrated networks (mean $\pm$ standard error over noise realizations).

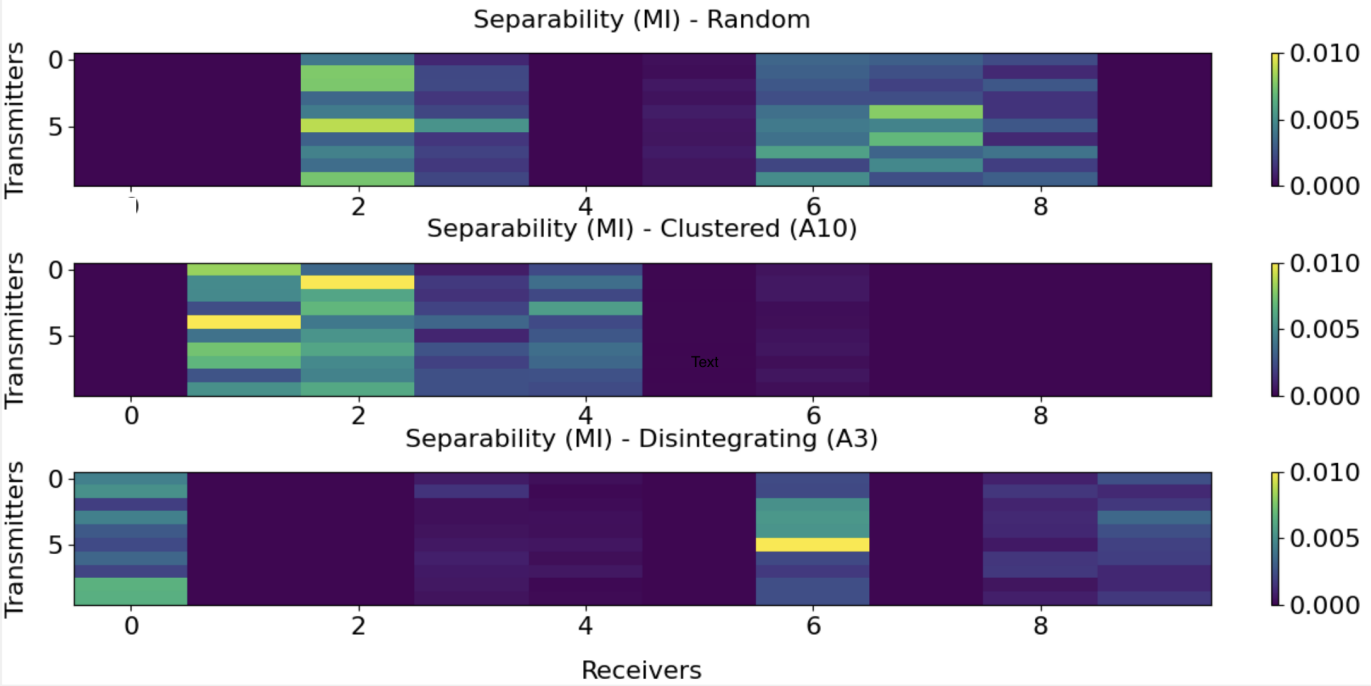

Fig. 4: Receiver-level separability matrices for (a) random, (b) clustered, and (c) disintegrated networks, computed at the mutual-information-maximizing lag under distance-based transmitter–receiver placement.

[9] M. T. Barros, "Capacity of the hierarchical multi-layered cortical microcircuit communication channel," in *Proceedings of the 5th ACM International Conference on Nanoscale Computing and Communication*, ser. NANOCOM '18. New York, NY, USA: Association for Computing Machinery, 2018.

[10] O. B. Akan, H. Ramezani, T. Khan, N. A. Abbasi, and M. Kuscu, "Fundamentals of molecular information and communication science," *Proceedings of the IEEE*, vol. 105, no. 2, pp. 306–318, 2017.

[11] M. Kuscu, E. Dinc, B. A. Bilgin, H. Ramezani, and O. B. Akan, "Transmitter and receiver architectures for molecular communications: A survey on physical design with modulation, coding, and detection techniques," *Proceedings of the IEEE*, vol. 107, no. 7, pp. 1302–1341, 2019.

[12] S. Lotter, M. T. Barros, R. Schober, and M. Schäfer, "Signal reception with generic three-state receptors in synaptic mc," in *GLOBECOM 2022 - 2022 IEEE Global Communications Conference*, 2022, pp. 4529–4534.

[13] M. Egan, M. Kuscu, M. T. Barros, M. Booth, A. Llopis-Lorente, M. Magarini, D. P. Martins, M. Schäfer, and P. Stano, "Toward interdisciplinary synergies in molecular communications: Perspectives from synthetic biology, nanotechnology, communications engineering and philosophy of science," *Life*, vol. 13, no. 1, 2023.

[14] T. Schreiber, "Measuring Information Transfer," *Physical Review Letters*, vol. 85, no. 2, pp. 461–464, 7 2000.

[15] S. P. Strong, R. Koberle, R. R. de Ruyter van Steveninck, and W. Bialek, "Entropy and Information in Neural Spike Trains," *Physical Review Letters*, vol. 80, no. 1, pp. 197–200, 1 1998.

[16] M. Veletić, M. T. Barros, I. Balasingham, and S. Balasubramaniam, "A molecular communication model of exosome-mediated brain drug delivery," in *Proceedings of the Sixth Annual ACM International Conference on Nanoscale Computing and Communication*, ser. NANOCOM '19. New York, NY, USA: Association for Computing Machinery, 2019.

[17] M. Veletić, M. T. Barros, H. Arjmandi, S. Balasubramaniam, and I. Balasingham, "Modeling of modulated exosome release from differentiated induced neural stem cells for targeted drug delivery," *IEEE Transactions on NanoBioscience*, vol. 19, no. 3, pp. 357–367, 2020.

[18] E. Izhikevich, "Simple model of spiking neurons," *IEEE Transactions on Neural Networks*, vol. 14, no. 6, pp. 1569–1572, 11 2003.

[19] E. M. Izhikevich, "Which model to use for cortical spiking neurons?" *IEEE Transactions on Neural Networks*, vol. 15, no. 5, pp. 1063–1070, 2004.

[20] C. Kayal, E. Moeendarbary, R. J. Shipley, and J. B. Phillips, "Mechanical response of neural cells to physiologically relevant stiffness gradients," *Advanced Healthcare Materials*, vol. 8, no. 18, p. 1901036, 2019.

[21] J. Lantoine, T. Grevesse, A. Villers, G. Delhaye, C. Mestdagh, M. Versaevel, D. Mohammed, C. Bruyère, L. Alaimo, S. P. Lacour, L. Ris, and S. Gabriele, "Matrix stiffness modulates formation and activity of neuronal networks of controlled architectures," *Biomaterials*, vol. 89, pp. 14–24, 2016.